Publication No. WI-2019-05
8 July 2019

The Watershed Institute

School of Natural Sciences
California State University
Monterey Bay
https://csumb.edu/watershed

100 Campus Center, Seaside, CA,
93955-8001
831 582 4696 / 4431

Central Coast Watershed Studies

CCoWS

Assessing steelhead passage and channel stability following dam removal on the Carmel River

Spring 2019

Mikaela Bogdan[1]
Katelyn Datan
Rene De La Fuente
David Nava
Rene Nunez
Madalyn Price[2]
Samantha Scalise[2]
Peter Vannerus
Trenton Westerson

Doug Smith (Ph.D.)[3]

[1]Chief Editor, [2]Editor, [3]Corresponding author: dosmith@csumb.edu

Executive Summary

San Clemente Dam was removed from the Carmel River in 2015. A new river channel was constructed to facilitate rainbow and steelhead trout movement through the site. The constructed channel was reorganized by high flows in 2017, leaving the possibility that barriers to fish migration had formed.

Fish passage was assessed at the former San Clemente dam site. The work was performed between the former dam location and a steep cascade located 160 m downstream of the mouth of San Clemente Creek in spring 2019 at a flow of 240 cfs. The study had three goals:

1) visual assessment of the channel for jumps greater than one foot, depths less than one foot, or widths less than three feet (AECOM 2018),
2) assessment of passage limited by high velocity (CalAm 2015),
3) assessment of channel stability by studying boulder transport.

Water depths and jump heights were assessed by on-site visual observations augmented by drone video. Velocity measurements were made using floats. Boulder stability was assessed by comparing boulder locations in geospatially referenced, drone-based orthophotos from before and after the 10-year flood of winter 2019.

Visual assessment indicated that no jump, depth, or width barriers were present at 240 cfs. Velocity measurements along two high gradient reaches found that both passable conditions and potentially impassible conditions existed at various times during the measurements at 240 cfs. Fifteen percent of 185 randomly selected boulders were transported (mean = 2 m) by the 10-year flow in winter 2019. The boulders are more stable now than they were in WY 2017.

Acknowledgements

California American Water provided access to the site and funding to purchase a real-time kinematic GPS drone.
Pat Iampietro provided technical support for drone missions.
Amy Pyle provided logistical support with field gear.

Disclaimer

This report was produced within the time and scope constraints of a semester-long undergraduate course at CSU Monterey Bay: River Hydrology (GEOL 460). It is a group senior thesis for the authors.

This report may be cited as:

Bogdan M, Datan K, De La Fuente R, Nava D, Nunez R, Price M, Scalise S, Vannerus P, Westerson T, Smith D. 2019. Assessing steelhead passage and channel stability following dam removal on the Carmel River. Watershed Institute, California State University Monterey Bay, Publication No. WI-2019-05, 31 pp.

Table of Contents

1 Introduction

In 1997 South-Central California Coast steelhead (*Oncorhynchus mykiss*) were listed as a federally threatened species (NMFS 1997). Dams and water diversions in the Carmel River have historically acted as stressors to anadromous steelhead and are cited as the primary causes of historically declining Carmel-run steelhead (NMFS 2002).

Dam removal is becoming an increasingly common practice in river restoration, but the environmental responses to dam removal are not well understood (Pizzuto 2002; East et al. 2015; Harrison et al. 2018). San Clemente dam, formerly located approximately 30 km (18.5 mi) upstream of the Pacific Ocean in the Carmel River watershed (Figure 1), was removed in 2015, and a new river channel was constructed. Specific objectives of the Carmel River Reroute and Dam Removal (CRRDR) project (Figure 2) included enhancement of habitat conditions for both resident rainbow trout and anadromous steelhead, and restoration of fish passage for steelhead (NMFS 2013; Boughton et al. 2016). To accomplish fish passage goals, an extensive step-pool system (Figure 3a,b) was created under the assumption that steps with a maximum height of one foot would provide optimal passage conditions for steelhead in both low and high flow conditions (CalAm 2015). Each step in the system was composed of five precisely placed, structurally-critical boulders approximately 1.5 m in diameter Marson et al. 2016).

A sub-two-year peak flow in 2016 caused unexpected movement of boulders (Marson et al. 2016). Following channel repairs in summer 2016, high flows spanning from 10 to 30-year floods (Figure 4) scattered most of the boulders and other large rocks used in the constructed channel in winter 2017 (Figure 3; Smith et al. 2017). It has been unclear how well anadromous steelhead would be able to navigate past the more random configuration of structural boulders in the river.

Fish passage studies must be performed at a variety of discharges to determine the range of flows that will allow steelhead migration given current channel conditions. A low-flow study in summer 2018 reported that the site was unpassable at 17 cfs, with approximately 50 specific impediments located and described (Smith et al. 2018). The original restoration design was created to allow fish passage at flows as low as 15 cfs, therefore present river geometry is significantly less capable of fostering fish migration. The 2018 report recommended assessing the site at higher flows and suggested that the new boulder configuration was relatively stable, as compared to the original design (Smith et al. 2018). Our study contributes to this work by assessing fish passage at a high-flow condition, and conducting the first assessment of boulder stability in the bed of the CRRDR channel.

In this report we assess stability of current boulder geometry and fish passage conditions at the CRRDR site (Figure 3) at approximately 240 cfs using a visual survey and low-altitude small unmanned aerial system (sUAS) photogrammetry and video. Water-year 2019 (WY19) experienced a 10-year flood event similar to those causing significant boulder movement in 2017. Although the WY 2017 peaks included two 10-year events followed by a 30-year event (Harrison et al 2018), direct observation indicated that many of the CRRDR boulder structures were reorganized in the first 10-year event of the winter. The following winter, WY18 had flows as high as the 2-year event, and did not significantly transport boulders. If boulders were reconfigured into stable structures in WY17, we would expect no difference in boulder location between WY17 and the peak flows of WY19.

As steelhead passage was one of the major objectives of the CRRDR project, the goals of our project are to determine if steelhead can navigate past the site given the current morphological conditions and high discharge, and to evaluate the potential for reconfiguration of present channel structure in future 10-year flood events.

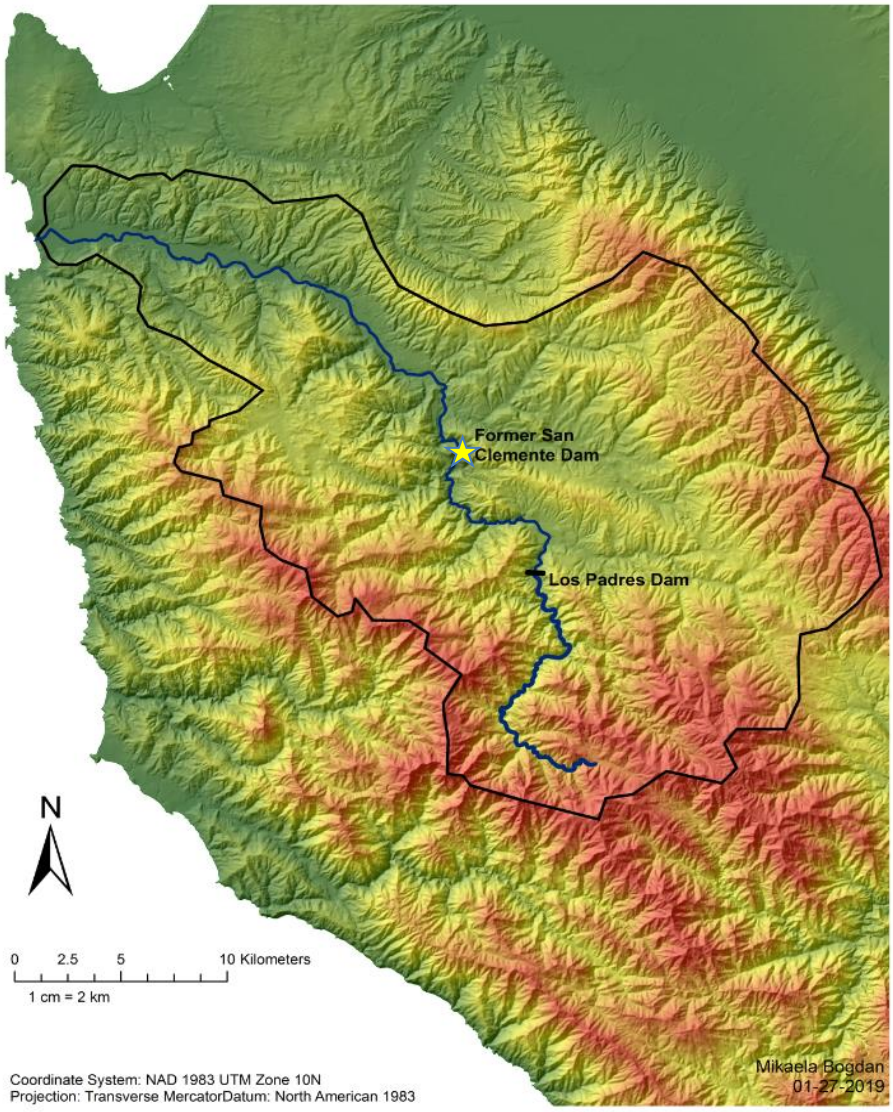

Figure 1. Location map of former San Clemente dam along the Carmel River (blue line). Carmel River watershed indicated by black polygon.

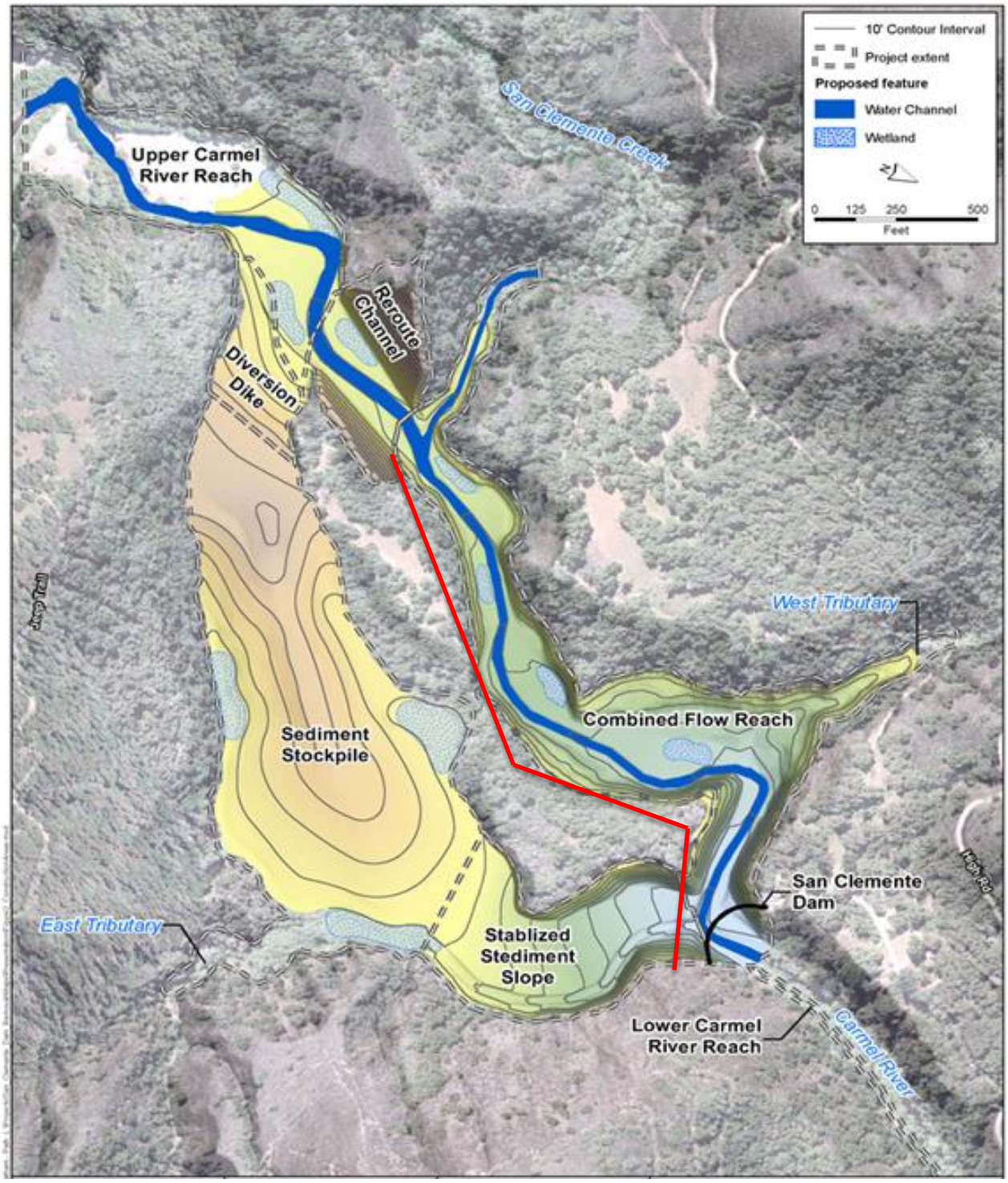

Figure 2. Map of the CRRDR project shows the Upper Carmel Reach, Reroute Reach, and Combined Flow Reach. Red line indicates regions with photogrammetry from March 28-29 2019 (figure modified from URS 2012; Marson et al. 2016).

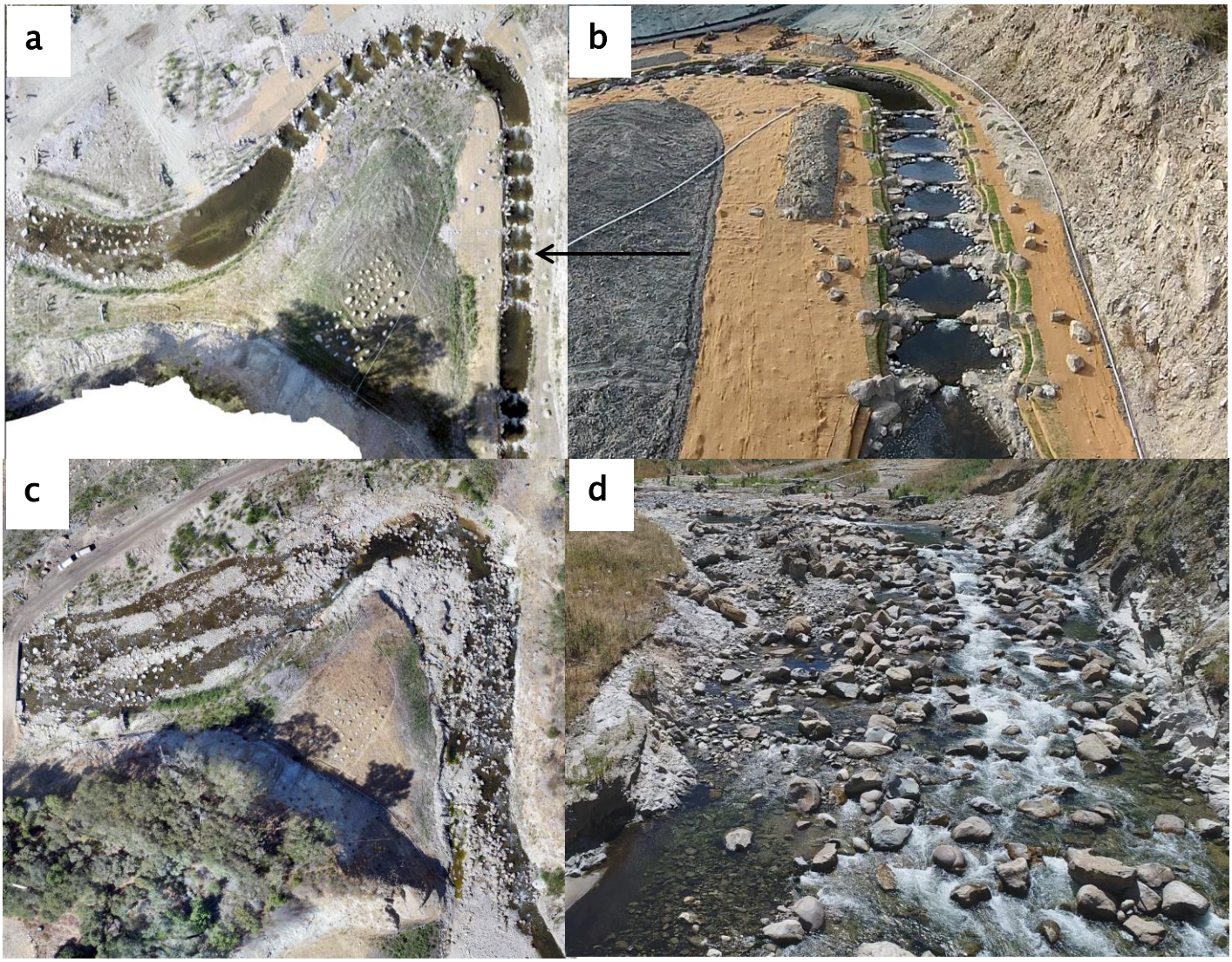

Figure 3. (a) sUAS orthophoto of downstream step-pool structures, resting pools and boulder field in 2016. (b) Oblique aerial photo taken in 2016 of downstream step-pools shown in figure 3a (indicated by arrow). (c) sUAS orthophoto of same downstream step-pool structures, resting pools and boulder field from Figure 3a after high flows and channel reconfiguration in WY17. (d) Oblique aerial photo of same step-pools from Figure 4b after high flows and channel reconfiguration in WY17.

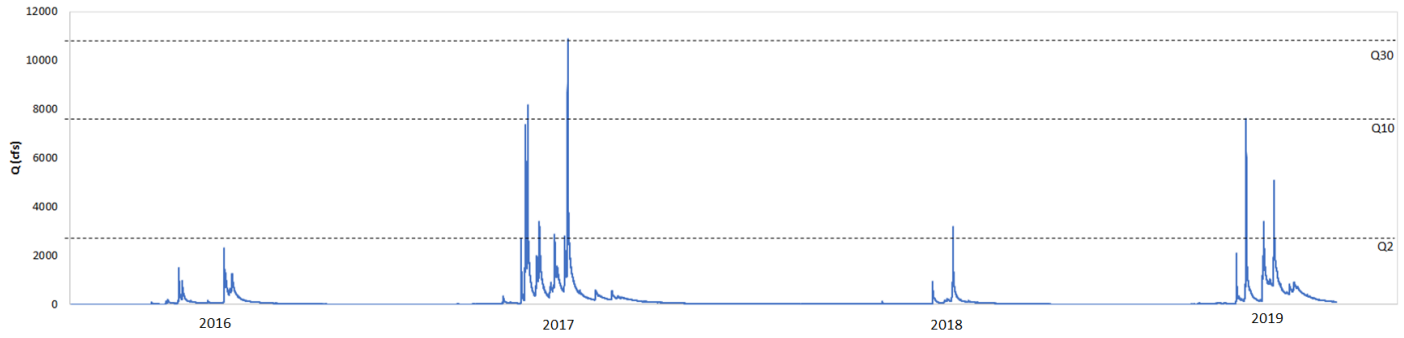

Figure 4. Instantaneous discharge for WY16 to present from the Robles del Rio stream gage. Calculated Q_2, Q_{10}, and Q_{30} are indicated by dashed lines. Q_{10} was event reached in both 2017 and 2019.

2 Methods

2.1 sUAS accuracy and precision

The project employed Phantom 4 Pro sUAS with real-time kinematic GPS (RTK) survey capabilities. The system captured low-altitude oblique video to augment the on-site visual assessment of fish passage and it was used to assess boulder mobility. We tested the system in two ways before use in the field. In section 2.1.1 we assess how well the system could reproduce 3D positions in DSMs and orthophotos. In section 2.1.2 we determine the threshold of horizontal motion of an object that can be detected by eye when observing time-series orhthophotos.

2.1.1 Assessing accuracy and precision of RTK sUAS

We conducted two separate flights in the same parking lot to assess accuracy and precision of the RTK sUAS. We set up the RTK base station on a known benchmark to get real-time corrections for drone position and flew a mission with the RTK sUAS at an altitude of 80 m. The resulting aerial photographs were processed in Pix4D to create both orthophotos and digital surface models (DSMs) for each flight. We used a Nikon three-second total station to collect accurate 3D coordinates of 30 points that would be easily seen in the orthophotos. We used a calculated correction factor to align the DSMs of both flights then created raster masks of each DSM, eliminating as much vegetation as possible to create digital elevation models (DEMs) for each flight using ArcMap (v. 10.5). We overlayed the two DEMs and calculated the elevation difference between the two aligned datasets. Rstudio software was used to conduct a two-sample t-test and to create boxplots to determine and convey between-survey precision of the RTK sUAS. To determine accuracy of the system, we compared the DEM from the flight and corresponding orthoimagery to vertical and horizontal

coordinates of total station points. The root mean square error (RMSE) between total station and sUAS data values were used to determine the accuracy of the photogrammetric products. We used the same methods for accuracy and precision analysis of RTK sUAS data collected at the study site except we used a Trimble R10 rover and base station to ground-truth the photogrammetry products.

2.1.2 Threshold level for detecting boulder movement

Boulder mobility was assessed by comparing boulder positions in a late 2018 orthophoto with the positions of the same boulders in an orthophoto produced after the 10-year flood of January 2019. We needed to determine the minimum boulder displacement that would be detectable in serial orthophotos. This section describes the methods of the test conducted to determine the threshold level for detecting boulder movement in orthoimagery.

We flew the RTK sUAS in an empty parking lot to determine a threshold level for detecting movement of objects on the ground from an elevation of 80 m. We conducted two flights with 15 small plates (0.18 m) and 15 large plates (0.26 m) placed on the ground in groups of four (Figure 5a). Each grouping of plates had a control which was not moved between flights and three study plates that were moved between flights by 4 cm, 8 cm, or 12 cm (Figure 5b,c). sUAS orthophotos from both flights were processed in Pix4D software and analyzed using ArcMap (v. 10.6) using the measure tool to measure apparent distance of plate movement in the orthophotos. The differences between measured movement and actual movement for each distance category (4 cm, 8 cm, and 12 cm) were calculated in Microsoft Excel and boxplots of the differences were created in Rstudio software.

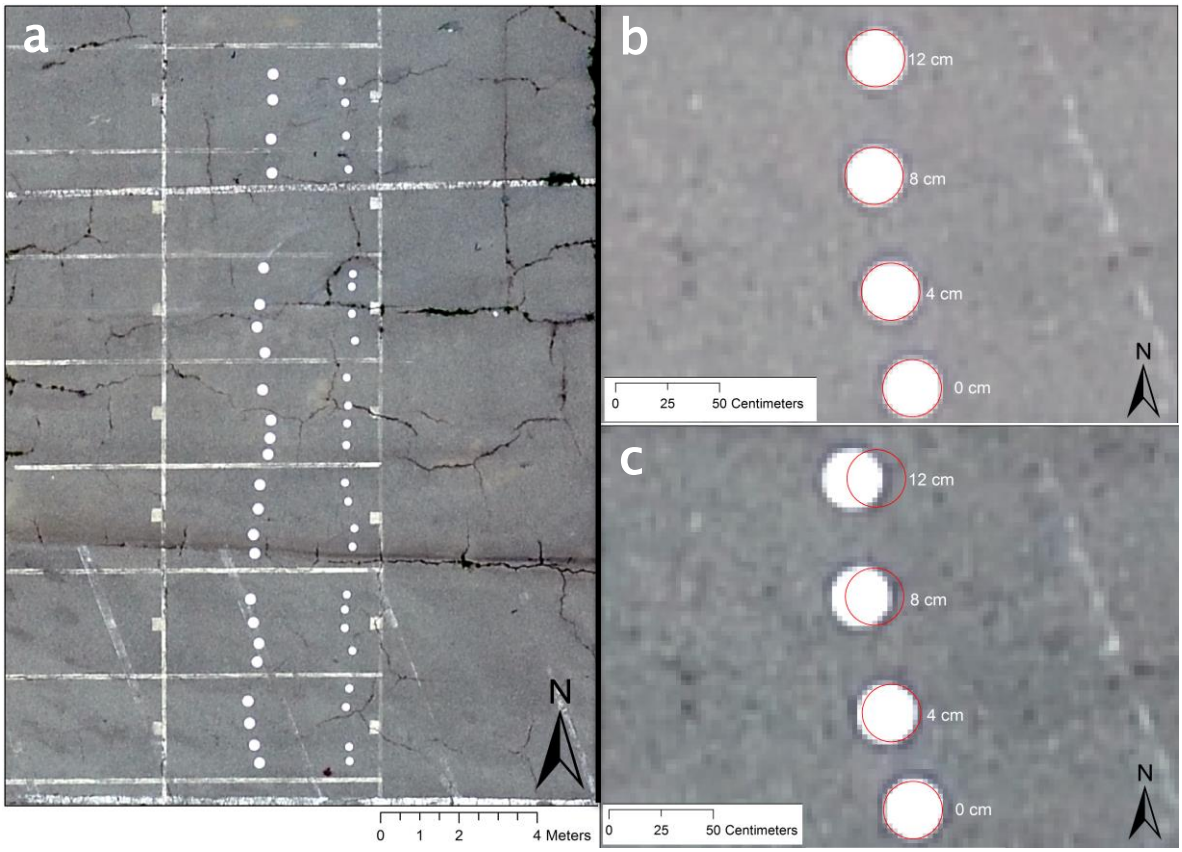

Figure 5. (a) sUAS orthophoto of all plates sampled. (b) sUAS imagery of initial plate positioning in one set of four of the 0.26 diameter plates. (c) Plates in same set of four, after being moved 0 cm, 4 cm, 8 cm, and 12 cm between flights.

2.1.3 sUAS photogrammetry and video on site

We flew the RTK sUAS at 80 m altitude to capture photogrammetry at the study site (Figure 2). A second Phantom 4 Pro sUAS without RTK GPS was flown along the same study reach and at specific areas of interest to capture aerial video. On-site flights were conducted at approximately 240 cfs on March 28 and 29, 2019 and photogrammetry was processed using Pix4D software. Video was used later to estimate surface water velocity.

2.2 Hydrology

We downloaded and plotted instantaneous discharge data from the 2016 water-year to present from the Robles Del Rio USGS stream gage website (USGS 2019). Although the Monterey Peninsula Management District Sleepy Hollow stream gage is close to the CRRDR site, the record is too short to calculate accurate flood recurrence intervals. Therefore data from the Robles Del Rio gage was downloaded as a proxy for Sleepy Hollow data, under the assumption that recurrence intervals (RIs) of peak floods at the Robles Del Rio gage are approximately the same for co-occurring peaks at the Sleepy Hollow gage. We prepared the data in Microsoft Excel and created a continuous hydrograph showing instantaneous (15-minute) discharges from October 1, 2015 (the start of the 2016 water year) to the present (April 1, 2019). We calculated the RI of various flood events (Q2, Q10, Q30, and Q50) using log-transformed Pearson Type-Three Frequency Analysis.

2.3 Fish passage

2.3.1 Visual Assessment

Potential barriers to fish passage were visually assessed by walking along the river banks on March 30, 2019 at a discharge of approximately 240 cfs and marking areas of concern on orthoimagery collected in previous surveys of the site. We used sUAS video and photogrammetry from the March 2019 flights to supplement on-site visual reconnaissance. We based our passage assessment on the following criteria presented in the CRRDR post-construction monitoring plan (AECOM 2018):

1. A potential barrier exists at a given cross section if the average depth is less than one foot or the width is less than three feet. If there are multiple passage corridors in the cross section, assess the one that is most conducive to passage.

2. A potential barrier exists where a hydraulic drop spans the wetted channel width, and the jump height exceeds one foot or the downstream launching pool is less than two feet deep. This is a potential barrier if jump behavior is required to pass the feature due to absence of an identifiable subsurface passage corridor.

All potential barriers fitting the AECOM (2018) criteria that were located along the most conducive passage route were documented using ArcMap (v.10.5) software with additional mapping of resting pools based on video of flow captured with the sUAS.

2.3.2 Velocity in three hydraulically distinct areas

We estimated velocity at three hydraulically and morphologically distinct reaches. The “upper rapids” reach represents a steep cascade (5% gradient) reach with larger steps. The “above lower rapids” reach represents a riffle reach with less gradient (2% gradient). The “lower rapids” reach is a narrow, steep reach (5% gradient) with small steps. These three sites were selected to represent the range of potential velocity barriers observed at 240 cfs (Figure 6). We used the float method (using oranges) for measuring velocity in these reaches because safety concerns prohibited use of current meters. Easily identifiable features in the sUAS videos were selected as starting and stopping points for the floats in each distinct reach. Timestamps on the sUAS videos were used to calculate the time it took each float to move from the designated starting point to the stopping point and the distances between starting and stopping points were measured from sUAS photogrammetry in ArcMap (v. 10.5). Video also illustrated natural resting points where eddying occurred. We calculated surface velocity for each hydraulically distinct reach by dividing the distance between starting and stopping points by the time taken for the float to move from start to finish. Surface velocity determined using floats overestimates the average velocity of the river by approximately 15%, so the surface velocities were multiplied by 0.85 to correct the error. A table of thresholds for steelhead passage at varying velocities over given distances was created in Microsoft Excel.

Figure 6. Upper rapids (left), above lower rapids and lower rapids (right) where floats were deployed and sUAS video was taken to estimate surface velocity.

2.4 Boulder structure mobility

We overlayed and examined orthoimagery from an 80-m mission flown in March 2019 using the RTK sUAS and an orthophoto from a similar 80-m sUAS mission flown in October 2018 to determine whether the two orthophotos were horizontally aligned. We then used a random number generator to determine placement of 21 transects along the river channel. Transects were drawn on the 2019 orthophoto (Figure 7). We identified every rock greater than or equal to approximately 0.3 meters that intersected the transect with a unique identification number. The rocks were measured across

their intermediate axis to determine size. The March 2019 and October 2018 orthophotos were compared to evaluate boulder movement between 2018 and 2019. Rocks that were identified in the 2018 orthophoto but could not be seen in the 2019 orthophoto were categorized as “missing”. Missing boulders were excluded from further data analysis because the fate of missing boulders (either buried or transported beyond our study reach) was indeterminate. Distance from the channel thalweg and net translational movement of identified boulders were measured and recorded. All measurements were done using ArcMap (v. 10.5). The thalweg position was determined from the longitudinal profile (long profile) conducted in October of 2018 using Spectra Precision EPOCH 50 RTK GPS rovers and base station.

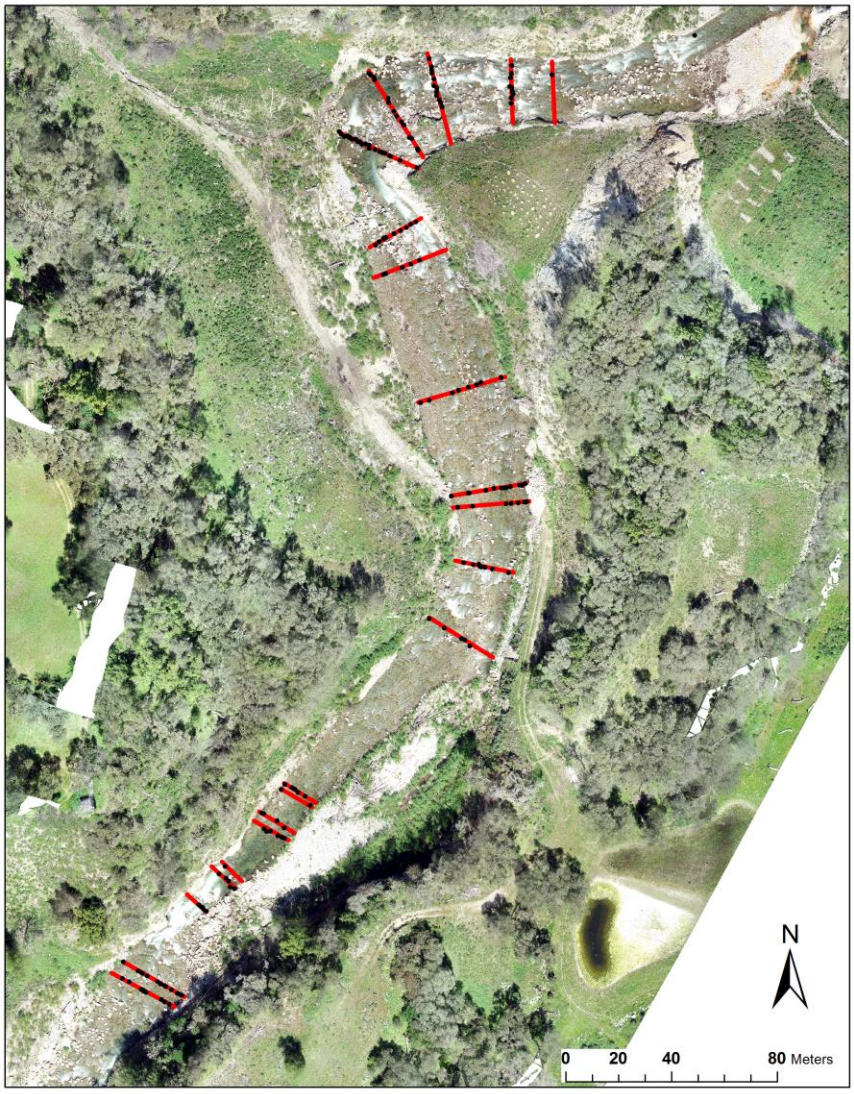

Figure 7. Transects used for boulder movement analysis drawn on 2019 orthophoto (red lines). Black dots represent boulders used in analysis.

Local slope for each transect was regressed from the 2018 long profile. The channel was broken up into sections based on similarity in slope for any given reach and transect locations were indicated on the profile (Figure 8). Slopes for transects 1-5 were calculated using distance and elevation values from a profile drawn in ArcMap (v. 10.6) because these transects either extended past the 2018 long profile or they were located along a reach where slope was oversimplified by collection of too few data points in the long profile. All slope values were used to conduct further statistical analysis.

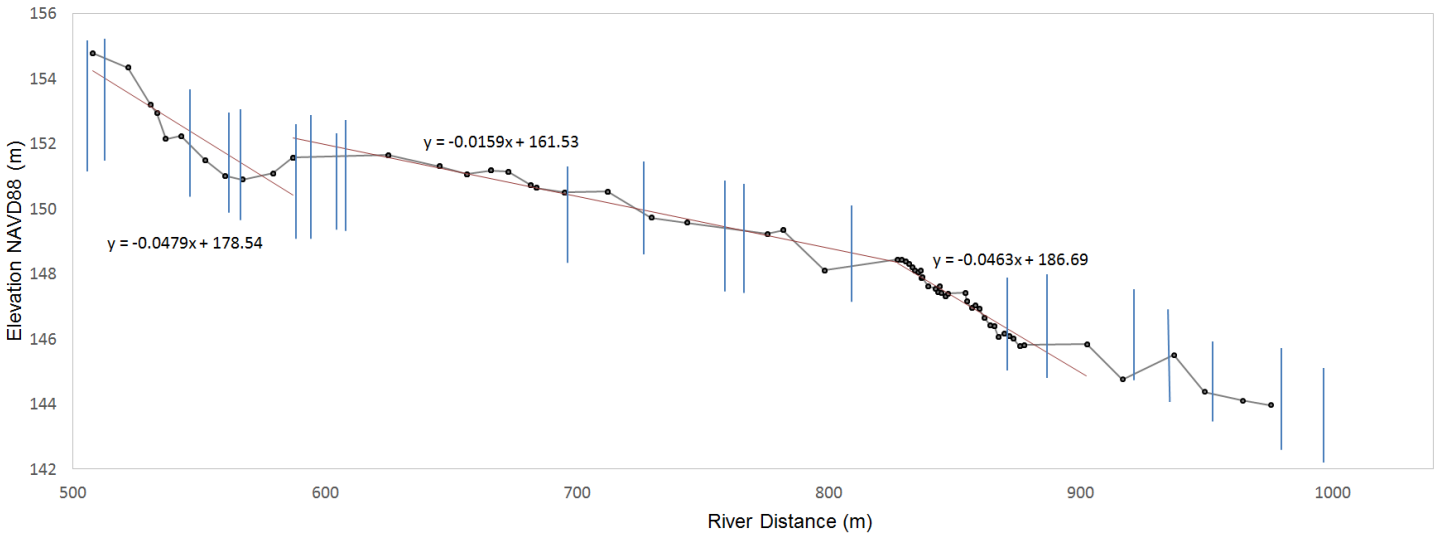

Figure 8. Longitudinal profile of study reach. Blue lines indicate locations of transects used for analyzing boulder movement. Trendlines are shown in red. Linear equations for each section of similar slopes are shown. Slopes for transects 1-5 (starting from downstream) were found using orthoimagery instead of regression and are therefore not shown on the long profile.

2.4.2 Statistical Analysis

We used local slope at each transect divided by distance from thalweg as a proxy for shear stress and created boxplots showing the relationship between shear stress and probability of boulder movement. We conducted a chi-square goodness-of-fit analysis to determine a relationship between likelihood of boulder movement and whether boulders were in a structure or isolated and we created a corresponding bar plot. We conducted a linear regression and created a scatter plot to assess distance of translational movement as a function of boulder size. We randomly subset 30unmoved boulders to create datasets with approximately equal frequencies of unmoved and moved data points to conduct two logistic regressions assessing probability of movement as a function of boulder size and probability of movement as a function of distance from the channel thalweg. All analyses and plots were done in Rstudio software.

3 Results

3.1 Photogrammetry data collection

3.1.1 Assessing accuracy and precision of RTK sUAS

Average horizontal error between orthophotos flown at 80 m and ground survey points was 0.017 m and 0.021 m for flights one and two respectively. Vertical errors were very high because the sUAS camera was not calibrated in the software (Table 1). A paired t-test between flight one and total station (TS) elevation values shows a significant p-value of 14E-04, based on a t-value of -4.204, and 58 degrees of freedom (df). A paired t-test between flight two and TS elevations also yields a significant p-value of 3E-04, based on a t-value of -3.9156, and df equal to 58 (Table 2). Paired t-tests comparing the horizontal values of the flights to the TS values show an insignificant p-values of 0.315 for flight one (t-value = -1.0 and df = 59), and 0.051 for flight two (t-value = 2.0 and df = 59) (Table 2).

Table 1. Horizontal and vertical accuracy assessment of flights one and two.

	Horizontal Error F1 (m)	Horizontal Error F2 (m)	Vertical Error F1 (m)	Vertical Error F2 (m)
Range	0.063	0.058	0.040	0.053
Mean	0.017	0.021	0.760	0.810
St Dev	0.015	0.015	0.011	0.011
RMSE	0.022	0.026	0.760	0.810

Table 2. Paired t-test comparing flight elevation values to TS elevation values.

		t-value	df	p-value
Vertical	Flight 1 vs TS	-4.2	58	1E-04
	Flight 2 vs TS	-3.9	58	3E-04
Horizontal	Flight 1 vs TS	-1.0	59	0.315
	Flight 2 vs TS	2.0	59	0.051

The average ground elevation difference between flights one and two was 0.05 m, with a standard deviation of 0.012, a range of 0.080 m, and a root mean square error (RMSE) of 0.052 m (Table 3). The average horizontal difference was 0.023 m, with a range of 0.057m, a standard deviation of 0.013 m, and a RMSE of 0.026 m. A paired t-test comparing the elevation values from these two flights resulted in a p-value of 1E-02 (t-value = -2.6 and df = 33). A paired t-test comparing the horizontal values from these two flights shows a significant p-value of 5E-03 (t-value = -2.9 and df = 59) (Table 4).

Table 3. Summary statistics of DEM elevation values and difference values between flights one and two.

	Horizonal Error (m)	Vertical Error (m)
Range	0.057	0.080
Mean	0.023	0.050
St Dev	0.013	0.012
RMSE	0.026	0.052

Table 4. Paired t-test comparing elevation values, and horizontal values between flights one and two.

	t-value	df	p-value
Vertical	-2.6	33	1E-02
Horizontal	-2.9	59	5E-03

3.1.2 Threshold level for detecting boulder movement

A boxplot of true plate offset and estimated error between true and measured distance of offset for all distances (4 cm, 8 cm, and 12 cm) of both large and small plates shows a maximum variability between all offset distances of ±1 cm. Median estimation error was least in plates that were moved 4 cm and 12 cm, while median estimation error of plates moved 8 cm was approximately -0.3 cm (Figure 9). Measurements of plates moved 4 cm and 8 cm tended to be underestimated while measurements of plates moved 12 cm were overestimated from the true displacement. Plate size does not appear to have an effect on detectability of movement, and no significant difference exists between the true offset and measured offset between and within displacement distance categories (Figure 9).

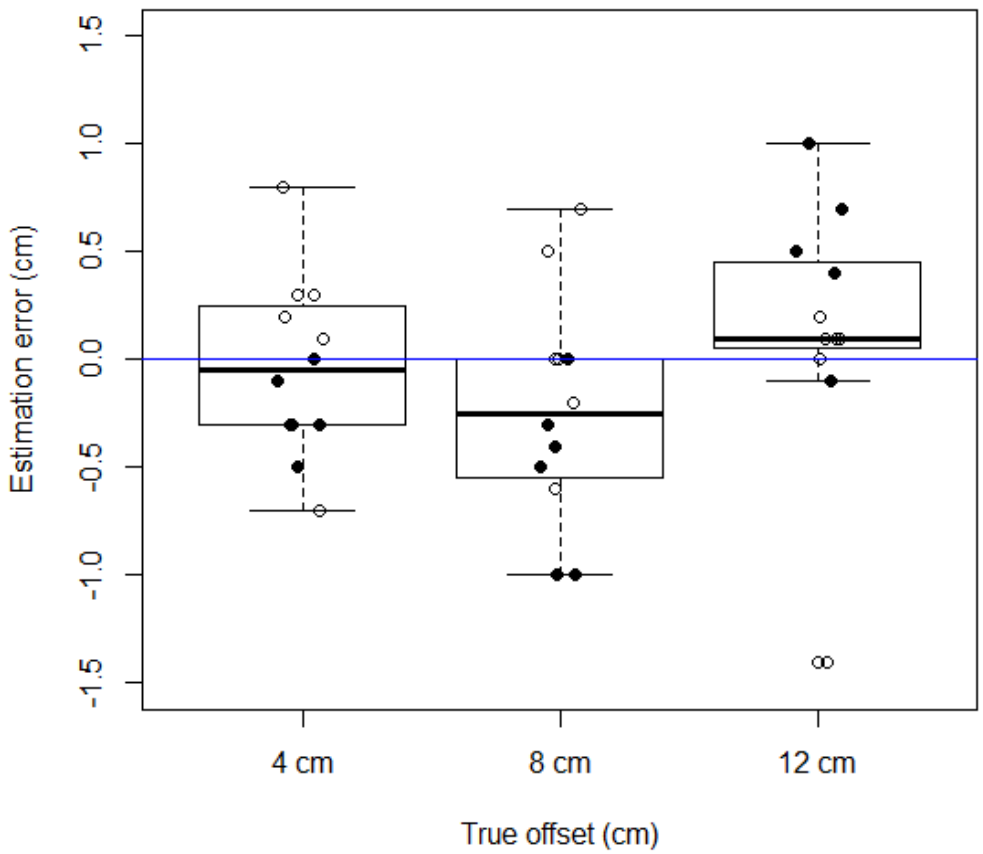

Figure 9. Boxplot showing true plate offset (4 cm, 8 cm, and 12 cm) and measured plate offset. Data points for large plates are indicated by black dots, data points for small plates are indicated by hollow circles. Blue line indicates a no difference between the actual and the measured data.

3.2 Fish Passage

Based on a direct visual assessment, low-altitude sUAS photogrammetry and sUAS video, fish passage does not appear to be impeded at 240 cfs. Two width barriers, three jumps greater than one foot, and one obstruction to flow were located, although none of the barriers identified were located along the most conductive migration route (Figures 10,11). In addition, resting pools were identified at 18 locations throughout the study reach, including high-velocity reaches of concern. Pools covered about 200 m^2, where average surface area of pools is roughly 11 m^2.

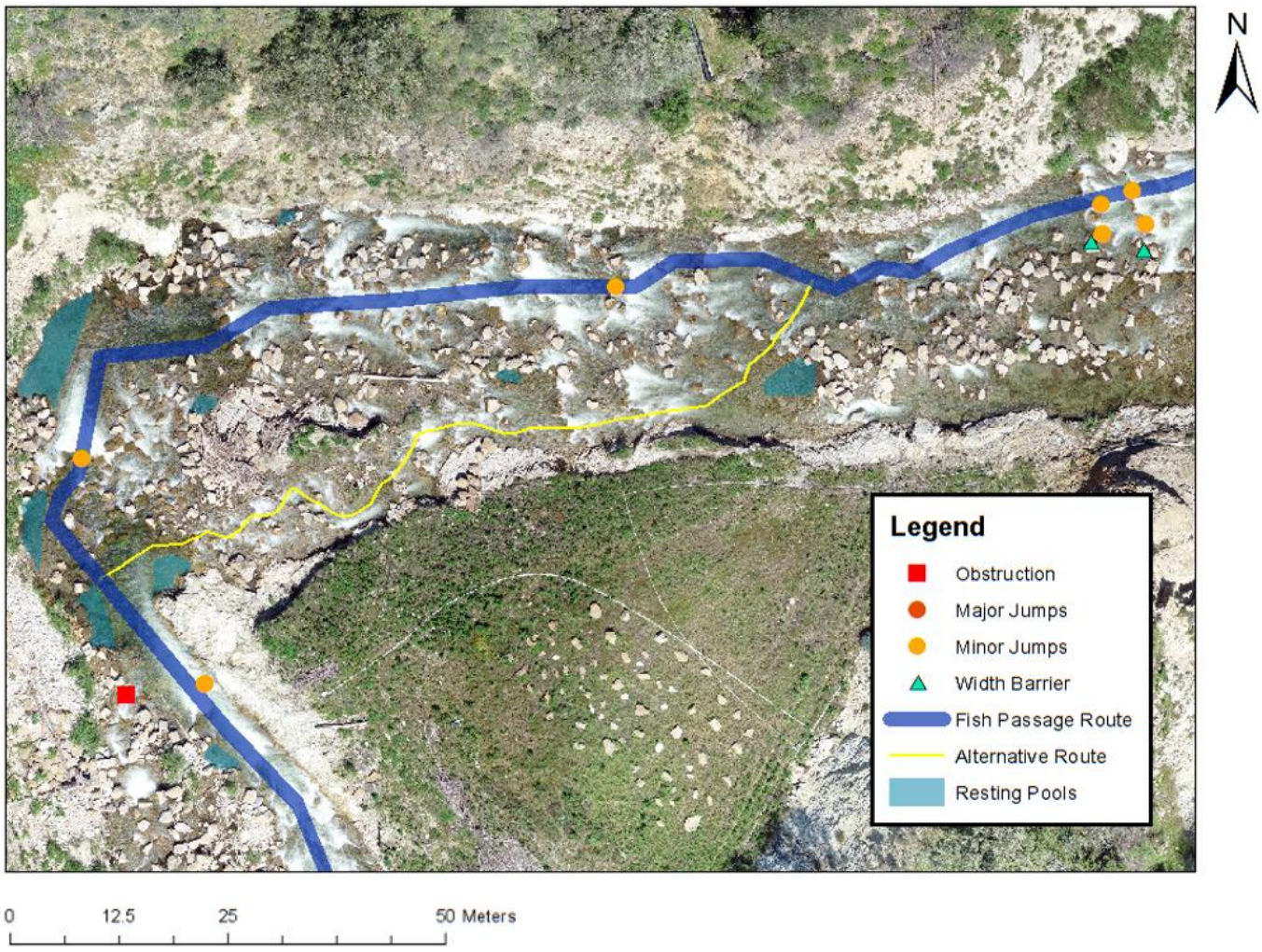

Figure 10. Fish passage assessment in lower reach with obstruction, potential passage impediments, most conductive route, alternative route and resting pools mapped on March 2019 orthophoto.

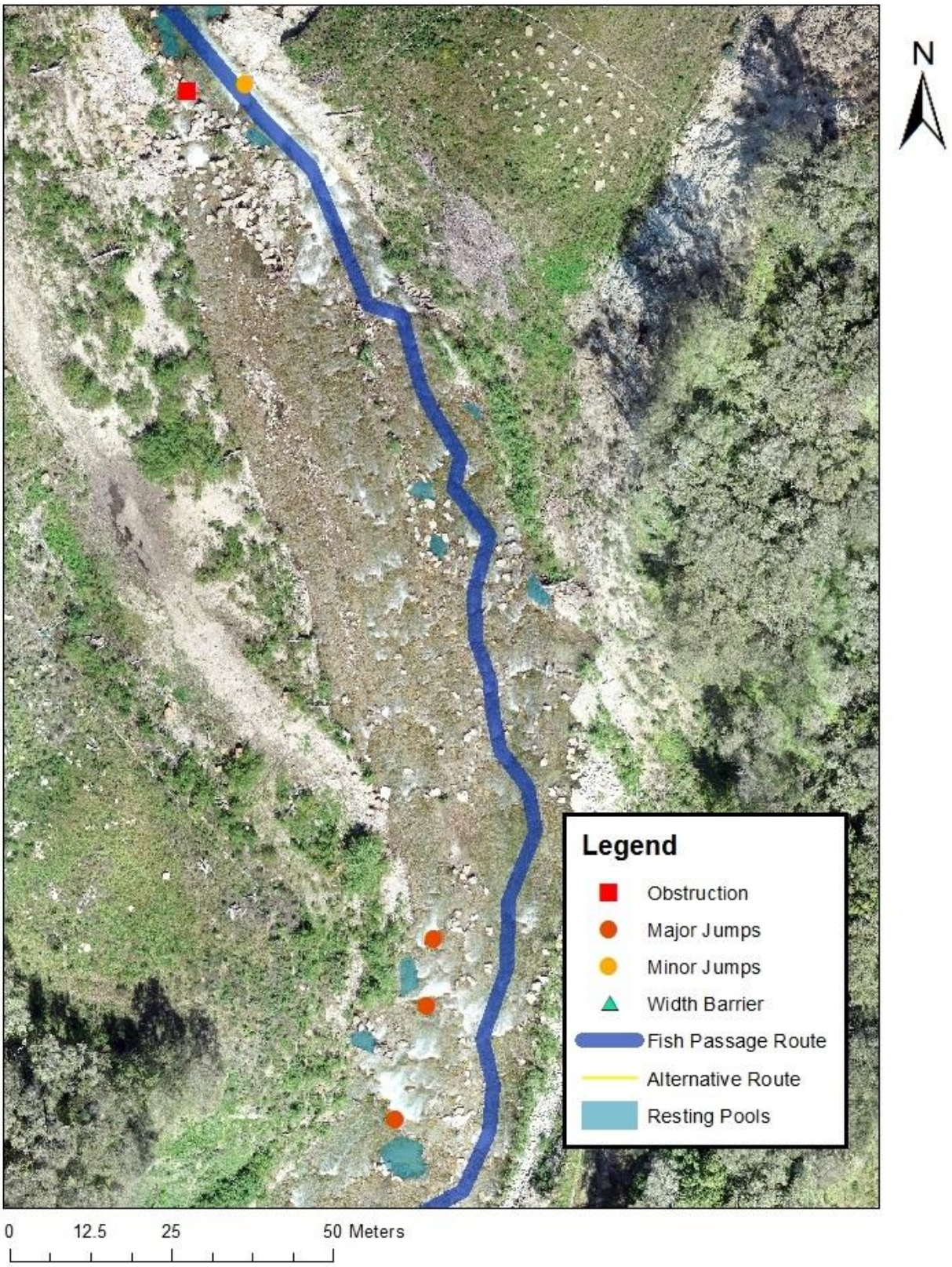

Figure 11. Fish passage assessment in upper reach with overlapping imagery of obstruction, minor jump, resting pool from the downstream reach (see Fig. 10), upstream potential passage impediments, most conductive route, and resting pools mapped on March 2019 orthophoto.

3.3 High Velocity

Average velocity in the upper rapids is 1.93 m/s and average velocity for the lower rapids is 2.06 m/s. The lower rapids high-gradient section has an average velocity of 2.18 m/s while the low-gradient part of the lower section has an average velocity of 1.98 m/s (Table 5). Table 6 shows velocity thresholds for steelhead passage. Number of trials using floats to estimate velocity in high gradient and low gradient rapids are indicated within colored cells. Ten trials fell within acceptable velocity and distance ranges and five trials were above the maximum velocity threshold for passage steelhead passage (Table 6).

Table 5. Velocities found for the upper and lower rapids, split into high and low gradient.

	Lower(m/s)	Upper(m/s)
High Gradient	**2.18**	**1.93**
Low Gradient	**1.98**	**NA**

Table 6. Velocity thresholds for steelhead passage for given distances. Numbers indicate the count of trials that fell in each category. Green cells indicate viable passage, yellow cells indicate maximum velocity that is still passable, and orange cells exceed the maximum velocity threshold. Categories are converted to metric from Engineering Design Requirements (CalAm, 2015)

	Distance (meters)				
m/s	< 18	18-30	31-61	62-91	>91
2.4					
2.1	1	1			
1.8	4	3			
1.5	2	3			
1.2		1			
0.9					
0.6					

3.4 Boulder Structure Mobility

We assessed the mobility of 185 boulders and found that 85% did not move between WY18 and WY19. Translational movement measured ranged from 0.5 m to 7 m with a mean distance of 2 m. Boxplots showing probability of movement as a function of a shear stress index indicate there is no significant impact of shear stress on probability of movement (Figure 12). Our index of shear stress used the cross-channel distance from the thalweg as a substitute for hydraulic radius. This substitution assumed that depth shallowed gradually between a maximum depth at the thalweg, and the water's edge. In the CRRDR, the channel does not generally shallow with distance from the thalweg, so the index is a weak approximation of shear stress.

Figure 12. Boxplot showing relationship between shear stress and probability of boulder movement. Slope/distance from thalweg was used as a proxy for shear stress.

We assessed whether boulder mobility depended on whether the boulder was isolated or adjacent to other boulders. A Chi-square analysis of the relationship between frequency of moved and unmoved boulders and whether boulders were found in a structure or isolated resulted in an insignificant p-value of 0.85 with df = 1 and a X-value of 0.038 The corresponding bar plot provides a visual of the Chi-square results, where the proportion of isolated moved boulders and moved boulders in a structure is approximately equal to the proportion of isolated unmoved boulders and unmoved boulders in a structure (Figure 13).

A linear regression assessing translational distance of boulder movement as a function of boulder size resulted in a p-value of 0.30 (df = 25, t-value = 1.043). The associated scatter plot shows the insignificant relationship between boulder size and distance of movement (Figure 14). A logistic regression of probability of movement as a function of boulder size resulted in a significant p-value

of 0.005 (df = 54, z-value = 2.780). The associated plot shows as boulder size increases the probability of movement also increases (Figure 15). A logistic regression of probability of movement as a function of distance from thalweg yielded a slightly insignificant p-value of 0.06 (df = 56, z-value = 1.894). The corresponding plot shows that as distance from the thalweg increases probability of movement also increases (Figure 16).

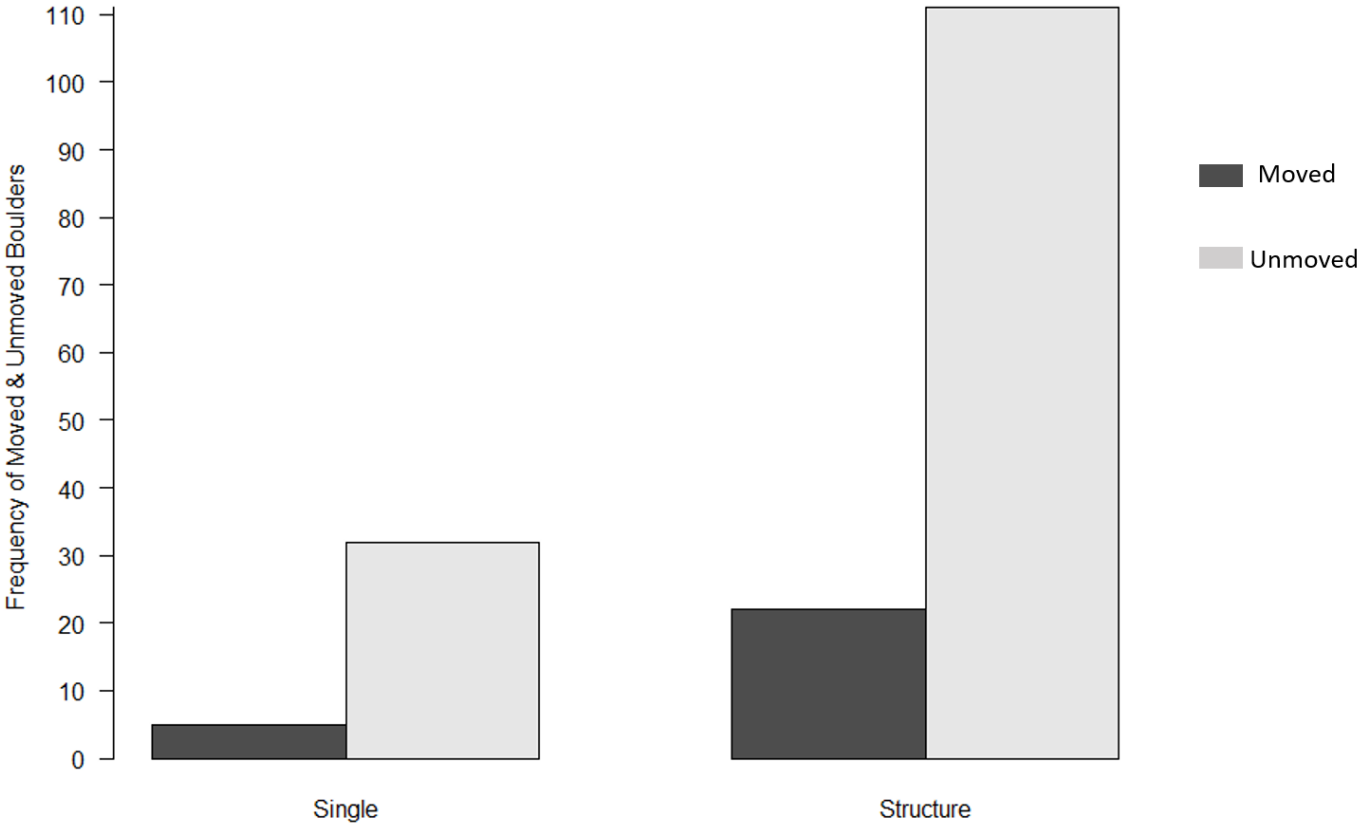

Figure 13. Bar plot visual of Chi-square analysis results of moved and unmoved boulders that were isolated, and moved and unmoved boulders that were in a structure.

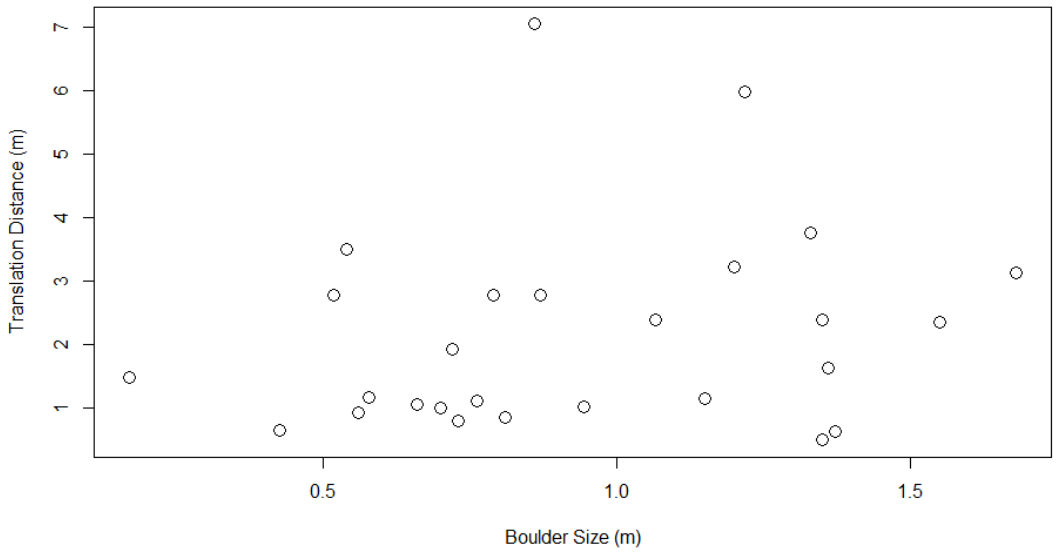

Figure 14. Scatter plot translational distance as a function of boulder size.

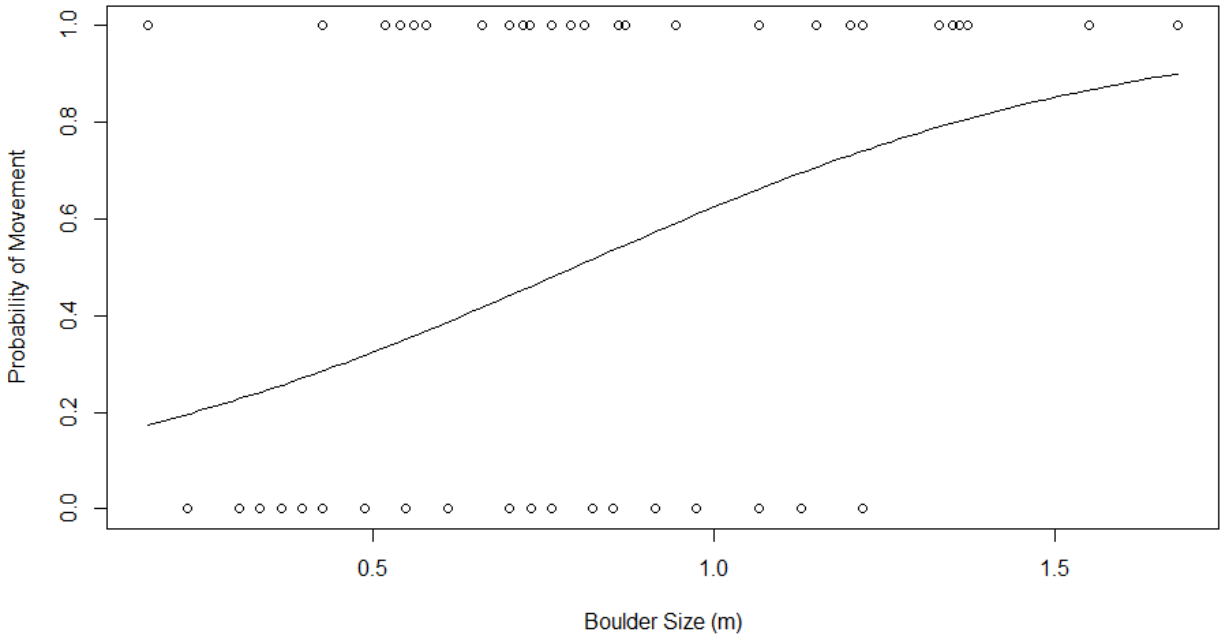

Figure 15. Logistic regression plot showing probability of movement as a function of boulder size. Open circles at the top of the plot indicate data points for boulders that moved and circles on the bottom of the plot indicate data points for boulders that did not move.

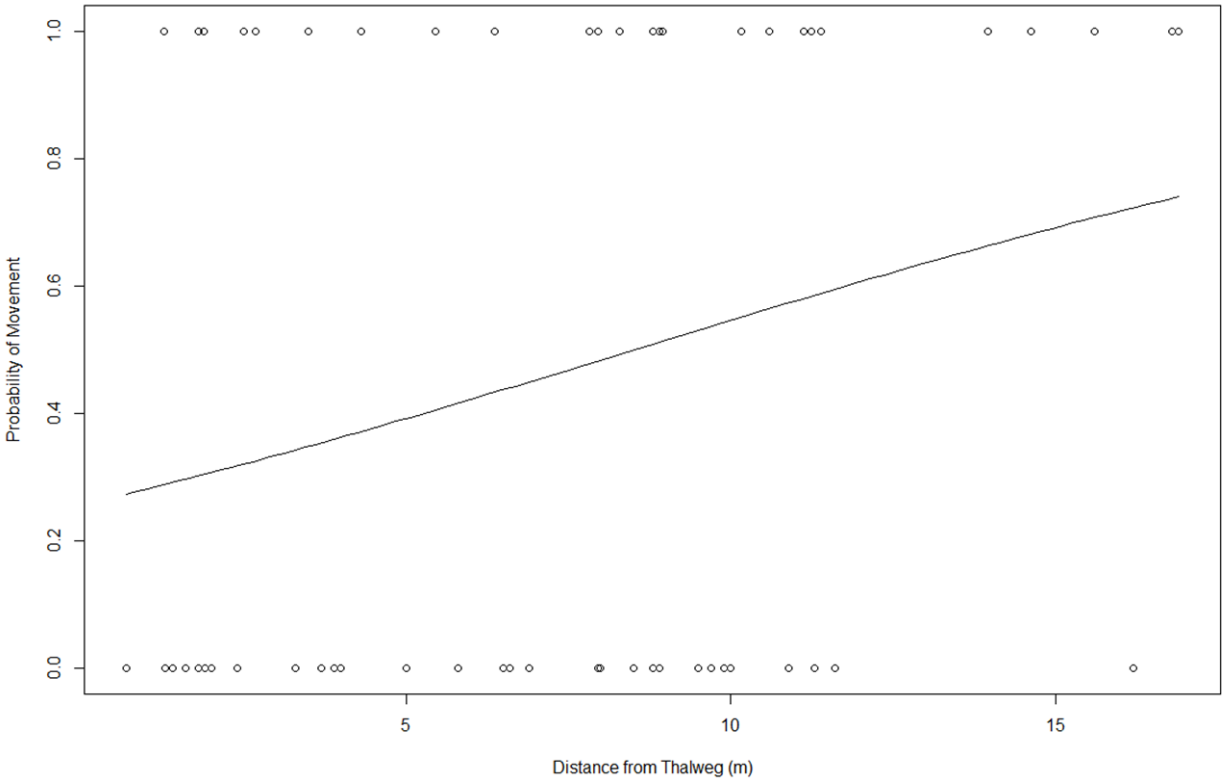

Figure 16. Logistic regression plot showing probability of movement as a function of distance from thalweg. Open circles at the top of the plot indicate data points for boulders that moved and circles on the bottom of the plot indicate data points for boulders that did not move.

4 Discussion

Potential barriers to fish passage were found at 17 cfs in summer 2018 (Smith et al. 2018). Our study, performed at 240 cfs, is the first to assess passage at a flow that is more typical of those encountered by winter-run steelhead in the Carmel River.

4.1 Fish Passage Impediments

We identify velocity as the only potential impediment to fish passage along the easiest passage route at 240 cfs in the reach between the former dam site and the cascade locate 160 m downstream from San Clemente Creek. In the study area velocity episodically exceeded the recommended velocity limits in the lower rapids (Table 6). Side eddies along this reach provide resting areas for steelhead to use periodically during passage through the high-velocity zone (Figure 11), improving the chances for passage.

4.2 Threshold level for detecting boulder movement

Boxplots showing the relationship between object displacement and the error of detecting that displacement show no significant difference between true offset and estimated offset (Figure 9) of plate movement for both large and small plates, and for all tested displacement distances (4 cm, 8 cm, 12 cm). Therefore, under ideal visual conditions, like those provided by white plates on a black pavement, we can easily detect displacement of 4 cm. Maximum variation for all distances was ± 1 cm from true displacement (Figure 9). Therefore, we find strong evidence supporting our use of RTK sUAS photogrammetry, obtained at resolution identical to the plate tests, for detecting boulder movement at the CRRDR project site.

4.3 Boulder structure mobility

The negative correlation between boulder size and probability of movement indicates that larger boulders are more likely than smaller boulders to move during high flows (Figure 15), consistent with Andrews (1983, 1994). Andrews (1983) results did not include boulder-sized sediment; our results suggest that the negative correlation extends into that larger grain size class. Neither our index of shear stress nor the presence of a boulder structure significantly influenced the likelihood of movement (Figures 16 and 19). Eighty-five percent of boulders analyzed did not move and movement of boulders was typically only 2 m among those that moved, suggesting the channel is relatively stable in the context of the 10-year flow event of 2019.

5 Conclusion

Based on our findings we conclude that no absolute barriers to steelhead migration exist along the study area at 240 cfs. Although the potential for future boulder movement and consequent formation of new impediments exists, the majority of the channel experienced no movement and movement was typically minor, suggesting the channel is less dynamic than in 2017. The continued migration of steelhead through the site in future years may prove critical for the proliferation of the species. Future studies at multiple discharges should be conducted to increase our understanding of steelhead passage through the current configuration of the channel under various hydraulic conditions.

6 References

AECOM. 2018. Carmel River Reroute and San Clemente Dam Removal Post-Construction Activity Plan, Habitat Monitoring & Reporting Plan. 66p.

Boughton DA, East A, Hampston L, Kiernan J, Leiker, S, Mantua N, Nicol C, Smith D, Urquhart K, Williams T, Harrison L. 2016. Removing a dam and re-routing a river: Will expected benefits for Steelhead materalize in Carmel River, California? NOAA Technical Memorandum, NOAA-TM-NMFS-SWFSC-553. US Department of Commerce. Southwest Fisheries Science Center, Santa Cruz, CA. 89 pp.

[CalAm] California American Water. 2015. Engineering Design Requirements for Carmel River Re-reoute and Dam Removal Project.

Marson L, Besson J, Biordi C, Conlen A, DeWolf K, Gravelle M, Hubbard H, MacSween L, Santos R, Sosa M, Thompson K, Trejo-Arce J, Smith D. 2016. First Year Assessment of the Carmel River Reroute and Dam Removal Project. Division of Science and Environmental Policy. Senior Thesis Report, 101 pp.
http://ccows.csumb.edu/pubs/reports/CCoWS_GEOL460_CarmelRiverRestorationYearOneAssess_160528.pdf

East AE, Pess GR, Bountry JA, Magirl CS, Ritchie AC, Logan JB, Randle TJ, Mastin MC, Minear JT, Duda JJ., Liermann MC., McHenry ML., Beechie TJ., Shafroth PB. 2015. Large-scale dam removal on the Elwha River, Washington, USA: River channel and floodplain geomorphic change. Geomorphology 246: 687-708.

Harrison, L.R., East, A.E., Smith, D.P., Logan, J.B., Bond, R., Nicol, C., Williams, T.H., Boughton, D.A., Chow, K. and Luna, L. 2018. River response to large-dam removal in a Mediterranean hydroclimatic setting: Carmel River, California, USA. Earth Surface Processes and Landforms, DOI: 10.1002/esp.4464. https://doi.org/10.1002/esp.4464..

[NMFS] National Marine Fisheries Service. 1997. Endangered and Threatened Species: Listing of Several Evolutionary Significant Units (ESUs) of West Coast Steelhead. Federal Register Notice: 62 FR 43937.

[NMFS] National Marine Fisheries Service. 2002. Instream flow needs for steelhead in the Carmel River: Bypass flow recommendations for water supply projects using Carmel River waters. 49pp.

[NMFS] National Marine Fisheries Service. 2013. Biological Opinion, The Carmel River Reroute and San Clemente Dam Removal Project at the San Clemente Dam on the Carmel River. National Marine Fisheries Service Southwest Region. North Central Coast Office, Tracking Number 2013/9633.

Pizzuto J. 2002. Effects of dam removal on river form and process. Bioscience 52: 683-691. DOI: Doi 10.1641/0006-3568(2002)052[0683:Eodror]2.0.Co;2

Smith, D., Chow, K., and Luna, L. 2017. Premature Mobility of Boulders in Constructed Step-pool River Structures in the Carmel River, CA: The Role of Fish-centric Design Constraints and Flow on Structural Stability. Abstracts with Program , AGU Fall Meeting, New Orleans.

Smith D., Bogdan, M., Klein J., and Terzoli, A. 2018. Carmel River Reroute and Dam Removal Fish Passage Assessment (Summer 2018). Watershed Institute, California State University Monterey Bay, Publication No. WI-2018-07, 43 pp. http://ccows.csumb.edu/pubs/reports/CCoWS_CRRDR_FishPassage_Summer2018_190402.pdf

[URS] 2012. Carmel River Reroute & San Clemente Dam Removal Project Indicative Channel Restoration Design: URS Corporation, 1 Montgomery St #900, San Francisco, CA 94104

[USGS] U.S. Geological Survey. 2019. USGS Current Conditions for the Nation. Robles Del Rio gage. https://waterdata.usgs.gov/nwis/uv?site_no=11143200.